TECHNICAL RESEARCH REPORT

Adaptive Identification and Control of Hysteresis in Smart Material Actuators

by Xiaobo Tan, John S. Baras

CDCSS TR 2003-3
(ISR TR 2003-40)

The Center for Dynamics and Control of Smart Structures (CDCSS) is a joint Harvard University, Boston University, University of Maryland center, supported by the Army Research Office under the ODDR&E MURI97 Program Grant No. DAAG55-97-1-0114 (through Harvard University). This document is a technical report in the CDCSS series originating at the University of Maryland.

Web site http://www.isr.umd.edu/CDCSS/cdcss.html

Adaptive Identification and Control of Hysteresis in Smart Material Actuators *

Xiaobo Tan and John S. Baras
Institute for Systems Research and
Department of Electrical and Computer Engineering
University of Maryland, College Park, MD 20742 USA
{xbtan, baras}@glue.umd.edu

Abstract

Hysteresis exhibited by smart materials hinders their wider applicability in actuators and sensors. In this paper methods are studied for recursive identification and adaptive inverse control of smart material actuators, where a Preisach operator with a piecewise uniform density function is used to model the hysteresis. Persistent excitation conditions for parameter convergence are discussed in terms of the input to the Preisach operator. Two classes of recursive identification schemes are explored, one based on the hysteresis output, the other based on the time difference of the output. Asymptotic tracking for the adaptive inverse control method is proved, and the condition for parameter convergence is given in terms of the reference trajectory. Practical implementation issues are also investigated. Simulation and experimental results based on a magnetostrictive actuator are used to illustrate the approach.

1 Introduction

Smart materials, e.g., magnetostrictives, piezoelectrics, and shape memory alloys (SMA), display coupling of elastomechanics with electromagnetic/thermal influences. Hence these materials have built-in sensing/actuation mechanisms. Hysteresis widely existing in smart materials, however, makes the effective use of smart material actuators and sensors quite challenging. Control of hysteresis in smart materials has attracted attention in recent years [1]. Hysteresis models can be roughly classified into physics-based models and phenomenological models. The most popular phenomenological hysteresis model used for smart materials has been the Preisach model [2, 3, 4, 5, 6, 7, 8]. A similar type of operator called Krasnosel'skii-Pokrovskii (KP) operator has also been used [9, 10].

Inverse compensation is a fundamental approach in coping with hysteresis, where one aims to cancel out the hysteresis effect by constructing a *right* inverse of the hysteresis operator [3, 11, 12, 10, 7, 8]. The performance of

*This research was supported by the Lockheed Martin Chair Endowment Funds.

inverse compensation is susceptible to model uncertainties and to errors introduced by (inexact) inverse algorithms. Hysteretic behaviors of smart materials often vary with time, temperature and some other ambient conditions. To combat this problem, a robust control framework was proposed by combining inverse compensation with l_1 control theory in [13]. An alternative approach is adaptive inverse control [11, 14, 15]. Tao and Kokotović developed an adaptive inverse control scheme for a class of hysteresis models with piecewise linear characteristics [11]. An adaptive identification and inverse compensation method was studied for the KP operator and applied to a SMA actuator by Webb *et al.* [14]. In [15] an adaptive inverse scheme was presented for piezoelectric actuators, where the Prandtl-Ishlinskii hysteresis operator was used for hysteresis modeling.

This paper is devoted to the study of recursive identification and adaptive inverse of hysteresis in smart materials. The following highlights the major differences of this work from the previous works reported in [11, 14, 15]: (1) the Preisach operator is used as the hysteresis model; (2) the persistent excitation (P.E.) conditions for the convergence of parameter identification are studied in terms of the input to the hysteresis operator; and (3) the asymptotic tracking property of the adaptive inverse control algorithm is proved, and the issue of parameter convergence is discussed in terms of the reference trajectory. Experimental results based on a magnetostrictive actuator, together with extensive simulation results, are used to examine the effectiveness of the proposed approach.

The remainder of the paper is organized as follows. The Preisach operator is briefly reviewed in Section 2. Recursive identification algorithms are studied in Section 3. Two classes of schemes are compared, one based on the output of the hysteresis model and the other based on the time difference of the output. The adaptive inverse control scheme is discussed in Section 4. Finally some conclusions are provided in Section 5.

2 The Preisach Operator

The Preisach operator is briefly reviewed in this section. A more detailed treatment can be found in [16, 17, 18]. For a pair of thresholds (β, α) with $\beta \le \alpha$, consider a simple hysteretic element $\hat{\gamma}_{\beta,\alpha}[\cdot,\cdot]$, as illustrated in Fig. 1. Let $C([0,T])$ denote the space of continuous functions on $[0,T]$. For $u \in C([0,T])$ and an initial configuration $\zeta \in \{-1,1\}$, $\omega = \hat{\gamma}_{\beta,\alpha}[u,\zeta]$ is a function from $[0,T]$ to $\{-1,1\}$ defined as follows [17]:

$$\omega(0) \triangleq \begin{cases} -1 & \text{if } u(0) \le \beta \\ \zeta & \text{if } \beta < u(0) < \alpha \\ 1 & \text{if } u(0) \ge \alpha \end{cases},$$

and for $t \in (0,T]$, setting $X_t \triangleq \{\tau \in (0,t] : u(\tau) = \beta \text{ or } \alpha\}$,

$$\omega(t) \triangleq \begin{cases} \omega(0) & \text{if } X_t = \emptyset \\ -1 & \text{if } X_t \neq \emptyset \text{ and } u(\max X_t) = \beta \\ 1 & \text{if } X_t \neq \emptyset \text{ and } u(\max X_t) = \alpha \end{cases}.$$

This operator is sometimes referred to as an *elementary Preisach hysteron* (it is called *hysteron* hereafter in this paper), since it is a building block of the Preisach operator. Define $\mathcal{P}_0 \triangleq \{(\beta,\alpha) \in \mathbb{R}^2 : \beta \le \alpha\}$. $\mathcal{P}_0$ is called the *Preisach plane*, and each $(\beta,\alpha) \in \mathcal{P}_0$ is identified with the hysteron $\hat{\gamma}_{\beta,\alpha}$. For $u \in C([0,T])$ and a Borel

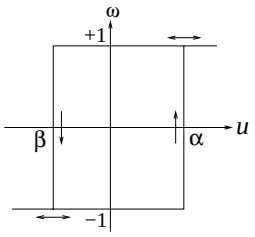

Fig. 1: An elementary Preisach hysteron $\hat{\gamma}_{\beta,\alpha}[\cdot,\cdot]$.

measurable initial configuration ζ_0 of all hysterons, $\zeta_0 : \mathcal{P}_0 \to \{-1, 1\}$, the output of the Preisach operator Γ is defined as [17]:

$$y(t) = \Gamma[u, \zeta_0](t) = \int_{\mathcal{P}_0} \mu(\beta, \alpha)\hat{\gamma}_{\beta,\alpha}[u, \zeta_0(\beta, \alpha)](t)d\beta d\alpha, \tag{1}$$

where the weighting function μ is often referred to as the *Preisach function* [16] or the *density function* [18]. Throughout the paper it is assumed that $\mu \geq 0$. Furthermore, to simplify the discussion, assume that μ has a compact support, i.e., $\mu(\beta, \alpha) = 0$ if $\beta < \beta_0$ or $\alpha > \alpha_0$ for some β_0, α_0. In this case it suffices to consider a finite triangular area in the Preisach plane $\mathcal{P} \triangleq \{(\beta, \alpha) \in \mathcal{P}_0 | \beta \geq \beta_0, \alpha \leq \alpha_0\}$ (see Fig. 2(a)).

The memory effect of the Preisach operator can be captured by the *memory curves* in $\mathcal{P}$. At time t, $\mathcal{P}$ can be divided into two regions:

$$\begin{aligned} \mathcal{P}_+(t) &\triangleq \{(\beta, \alpha) \in \mathcal{P} | \text{ output of } \hat{\gamma}_{\beta,\alpha} \text{ at } t \text{ is } +1\}, \\ \mathcal{P}_-(t) &\triangleq \{(\beta, \alpha) \in \mathcal{P} | \text{ output of } \hat{\gamma}_{\beta,\alpha} \text{ at } t \text{ is } -1\}. \end{aligned}$$

Now assume that at some initial time t_0, the input $u(t_0) = u_0 < \beta_0$. Then the output of every hysteron is -1. Therefore $\mathcal{P}_-(t_0) = \mathcal{P}$, $\mathcal{P}_+(t_0) = \emptyset$ and this corresponds to the "negative saturation" (Fig. 2(b)). Next assume that the input is monotonically increased to some maximum value at t_1 with $u(t_1) = u_1$. The output of $\hat{\gamma}_{\beta,\alpha}$ is switched to $+1$ as the input $u(t)$ increases past α. Thus at time t_1, the boundary between $\mathcal{P}_-(t_1)$ and $\mathcal{P}_+(t_1)$ is the horizontal line $\alpha = u_1$ (Fig. 2(c)). Next assume that the input starts to decrease monotonically until it stops at t_2 with $u(t_2) = u_2$. It's easy to see that the output of $\hat{\gamma}_{\beta,\alpha}$ becomes -1 as $u(t)$ sweeps past β, and correspondingly, a vertical line segment $\beta = u_2$ is generated as part of the boundary (Fig. 2(d)). Further input reversals generate additional horizontal or vertical boundary segments.

From the above illustration, each of $\mathcal{P}_-$ and $\mathcal{P}_+$ is a connected set [16], and the output of Γ is determined by the boundary between $\mathcal{P}_-$ and $\mathcal{P}_+$ if there is no Preisach weighting *mass* (or impulse in μ) on the curve. The boundary is called *the memory curve*. The memory curve has a staircase structure and its intersection with the line $\alpha = \beta$ gives the current input value. The *set of all memory curves* is denoted Ψ. The memory curve ψ_0 at $t = 0$ is called the *initial memory curve* and it represents the initial condition of the Preisach operator. Hereafter the initial memory curve will be put as the second argument of the Preisach operator.

Rate-independence is one of the fundamental properties of the Preisach operator:

Theorem 2.1 (Rate-independence) *[17] If $\phi : [0, T] \to [0, T]$ is an increasing continuous function satisfying $\phi(0) = 0$ and $\phi(T) = T$, then for $u \in C([0, T])$, $\Gamma[u \circ \phi, \psi_0](t) = \Gamma[u, \psi_0](\phi(t))$, $\forall t \in [0, T]$, where "$\circ$" denotes composition of functions.*

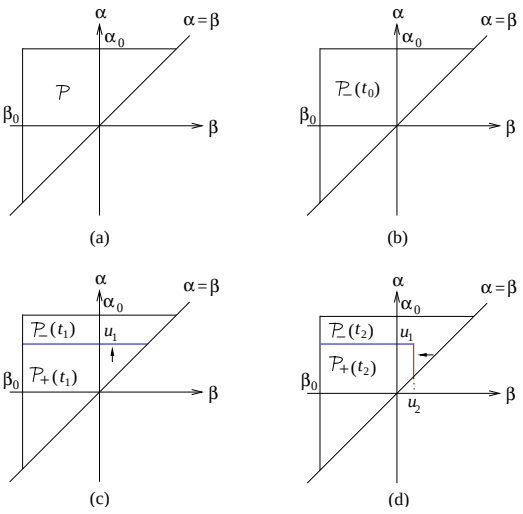

Fig. 2: Memory curves in the Preisach plane.

3 Recursive Identification of Hysteresis

For the Preisach operator, the "parameter" is the Preisach density function. A classical method to identify the density function is using the so called *first order reversal curves*, detailed in Mayergoyz [16]. A first order reversal curve can be generated by first bringing the input to β_0, followed by a monotonic increase to α, then a monotonic decrease to β. The term "first order reversal" comes from that each of these curves is formed after the first reversal of the input. Denote the output value as $f(\beta, \alpha)$ when the input reaches β. Then the density $\mu(\beta, \alpha)$ can be obtained as $\mu(\beta, \alpha) = \frac{1}{2}\frac{\partial^2 f(\beta,\alpha)}{\partial\beta\partial\alpha}$. Since it involves twice differentiation, a smooth approximating surface is fit to the data points in practice [3, 6]. As pointed out in [6], deriving the density by differentiating a fitted surface is inherently imprecise, since different types of approximating functions lead to quite different density distributions. A second approach is to devise the input sequence carefully and derive the Preisach weighting masses (on a discretization grid) directly from the output measurements [19]. This scheme is very sensitive to measurement noises as one can easily see. Hence a third approach is to identify the Preisach weighting masses or the weights for basis functions based on the least squares method [9, 10, 7]. All of the aforementioned methods are used off-line. However, it has been observed that the hysteretic behaviors of smart materials are dependent on temperature and some other ambient conditions, and often vary with time slowly. Hence it is desirable to have recursive, on-line schemes for the identification of hysteresis parameters.

3.1 Discretization of the Preisach operator

In practice the Preisach operator needs to be discretized in one way or another during the identification process. A natural way to approximate a Preisach operator is to assume that inside each cell of the discretized Preisach plane, the Preisach density function is constant. This approximation has nice convergence (to the true Preisach operator) properties under mild assumptions [19].

Let $[u_{min}, u_{max}]$ be the practical input range to the hysteresis operator, which is often a strict subset of $[\alpha_0, \beta_0]$.

For the hysteretic behavior one can focus on the triangle bounded by u_{min} and u_{max} in the Preisach plane, since the contribution to the output from hysterons outside this triangle is constant [7]. Discretize $[u_{min}, u_{max}]$ uniformly into $L+1$ levels (called *discretization of level* L in this paper), where the discrete input levels u_i, $1 \le i \le L+1$, are defined as

$$u_i = u_{min} + (i-1)\Delta_u,$$

where $\Delta_u = \frac{u_{max}-u_{min}}{L}$. The cells in the discretization grid are labeled, as illustrated in Fig 3(a) for the case of $L = 4$.

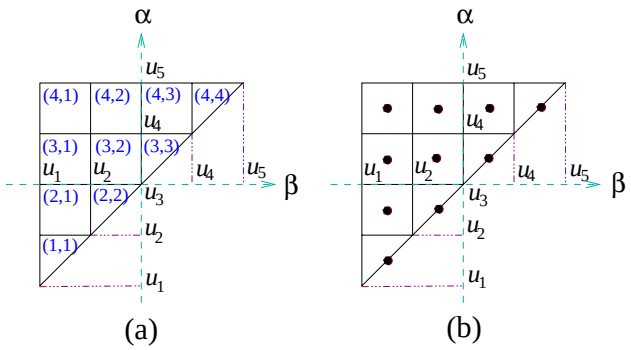

Fig. 3: Illustration of the discretization scheme ($L = 4$): (a) Labeling of the disretization cells; (b) Weighting masses sitting at the centers of cells.

We note that the Preisach operator with piecewise uniform density is still an infinite-dimensional operator. If one assumes that the Preisach weighting function inside each cell is concentrated at the center as a weighting mass (Fig. 3(b)), the corresponding Preisach operator becomes a weighted combination of a finite number of hysterons.

3.2 Recursive identification schemes

In the interest of digital control, the discrete-time setting is considered in this paper. One way to obtain a piecewise uniform density is to first identify the discrete weighting masses (Fig. 3(b)), and then distribute each mass uniformly over the corresponding cell [13]. A Preisach operator with discrete weighting masses is easier to analyze than a Preisach operator with a piecewise uniform weighting density; however, these two types of operators bear much similarity and essential results for one can be easily translated into those for the other. Hence recursive identification of Preisach weighting masses is first studied, and then the extension needed for identifying the density directly is briefly discussed.

In this paper two classes of identification algorithms are examined, one based on the hysteresis output, and the other based on the time difference of the output (called *difference-based* hereafter).

Output-based identification

The output $y[n]$ of the discretized Preisach operator (corresponding to the case illustrated in Fig. 3(b)) at time instant n can be expressed as

$$y[n] = \sum_{i=1}^{L} \sum_{j=1}^{i} \bar{W}_{ij}[n] \bar{\nu}^*_{ij}, \tag{2}$$

where $\bar{W}_{ij}[n]$ denotes the state (1 or -1) of the hysteron in cell (i, j) at time n, and $\bar{\nu}^*_{ij}$ denotes the hysteron's Preisach weighting mass. Stacking $\bar{W}_{i,j}[n]$ and $\bar{\nu}^*_{i,j}$ into two vectors, $W[n] = [W_1[n] \cdots W_K[n]]^T$ and $\nu^* = [\nu^*_1 \cdots \nu^*_K]^T$, where $K = \frac{L(L+1)}{2}$ is the number of cells, one rewrites (2) as

$$y[n] = \sum_{k=1}^{K} W_k[n] \nu^*_k = W[n]^T \nu^*. \tag{3}$$

Let $\hat{\nu}[n] = [\hat{\nu}_1[n] \cdots \hat{\nu}_K[n]]^T$ be the estimate of ν^* at time n, and let

$$\hat{y}[n] = \sum_{k=1}^{K} W_k[n] \hat{\nu}_k[n] = W[n]^T \hat{\nu}[n]$$

be the predicted output based on the parameter estimate at time n. The gradient algorithm [20] to update the estimate is

$$\hat{\nu}[n+1] = \hat{\nu}[n] - \gamma \frac{(\hat{y}[n] - y[n]) W[n]}{W[n]^T W[n]}, \tag{4}$$

where $0 < \gamma < 2$ is the adaptation constant. To ensure that the weighting masses are nonnegative, we let $\hat{\nu}_k[n+1] = 0$ if the k-th component of the right hand side of (4) is negative. Since this parameter projection step brings the parameter estimate closer to the true values, it does not invalidate the convergence result should this step were absent [20]. Hence this step will not be explicitly considered for convergence analysis in this paper (in particular, in the proof of Theorem 4.1). Define the parameter error $\tilde{\nu}[n] \triangleq \hat{\nu}[n] - \nu^*$. Then

$$\tilde{\nu}[n+1] = F[n] \tilde{\nu}[n], \tag{5}$$

where $F[n] = \mathbb{I}_K - \frac{W[n]W[n]^T}{W[n]^T W[n]}$, and $\mathbb{I}_K$ represents the identity matrix of dimension K.

It is well-known [20] that the convergence of the algorithm (4) depends on the *persistent excitation* (P.E.) condition of the sequence $W[n]$. The sequence $W[n]$ is persistently exciting if, there exist an integer $N > 0$ and $c'_1 > 0, c'_2 > 0$, such that for any n_0,

$$c'_1 \mathbb{I}_K \leq \sum_{n=n_0}^{n_0+N-1} \frac{W[n]W[n]^T}{W[n]^T W[n]} \leq c'_2 \mathbb{I}_K. \tag{6}$$

Due to the equivalence of uniform complete observability under feedback [20, 21], from (6), there exist $c_1 > 0, c_2 > 0$ such that for any n_0,

$$c_1 \mathbb{I}_K \leq G_N(n_0) \leq c_2 \mathbb{I}_K, \tag{7}$$

where $G_N(n_0)$ is the observability grammian of the system (5) defined as

$$G_N(n_0) = \sum_{n=n_0}^{n_0+N-1} \frac{\Phi[n, n_0]^T W[n] W[n]^T \Phi[n, n_0]}{W[n]^T W[n]},$$

and $\Phi[n, n_0]$ is the state transition matrix $\Phi[n, n_0] = \prod_{k=n_0}^{n-1} F[k]$. It can be shown [20] that when (7) is satisfied,

$$\|\tilde{\nu}[n+N]\| \leq \sqrt{1-c_1}\|\tilde{\nu}[n]\|, \tag{8}$$

from which exponential convergence to ν^* can be concluded.

Difference-based identification

An alternate way to identify ν^* is using the time difference $z[n]$ of the output $y[n]$, where

$$z[n] \stackrel{\triangle}{=} y[n] - y[n-1] = (W[n] - W[n-1])^T \nu^*.$$

Let $\hat{y}[n^-]$ and $\hat{y}[n-1]$ be the output predictions at time n and $n-1$ based on $\hat{\nu}[n-1]$, respectively, i.e.,

$$\hat{y}[n^-] \stackrel{\triangle}{=} W[n]^T \hat{\nu}[n-1],\ \hat{y}[n-1] \stackrel{\triangle}{=} W[n-1]^T \hat{\nu}[n-1].$$

Define $\hat{z}[n] \stackrel{\triangle}{=} \hat{y}[n^-] - \hat{y}[n-1] = (W[n] - W[n-1])^T \hat{\nu}[n-1]$. Let $V[n]$ be the time difference of hysteron states, $V[n] \stackrel{\triangle}{=} W[n] - W[n-1]$. Then we can obtain the following identification scheme based on $z[n]$:

$$\hat{\nu}[n+1] = \begin{cases} \hat{\nu}[n] - \gamma \frac{(\hat{z}[n] - z[n])V[n]}{V[n]^T V[n]}, & \text{if } V[n] \neq 0 \\ \hat{\nu}[n] & \text{if } V[n] = 0 \end{cases}. \tag{9}$$

As in the output-based scheme, an additional parameter projection step will be applied if any component of $\hat{\nu}[n+1]$ is negative. Similarly one can write down the error dynamics equation, the P.E. condition on $V[n]$, and the convergence rate estimate corresponding to the difference-based scheme (9). The sequences $V[n]$ and $W[n]$ are almost equivalent in the sense that, for any $N > 0$, $\{V[n]\}_{n=1}^N$ can be constructed from $\{W[n]\}_{n=0}^N$, and conversely, $\{W[n]\}_{n=1}^N$ can be constructed from $W[0]$ and $\{V[n]\}_{n=1}^N$. However, there are motivations to introduce the difference-based scheme (9). While $W[n]$ has components ± 1, the components of $V[n]$ are ± 2 or 0. Often times most components of $V[n]$ are 0 since $V_k[n] \neq 0$ only if the k-th hysteron changed its state at time n. This has two consequences: (1) The P.E. condition of $V[n]$ is easier to analyze than that of $W[n]$; (2) The convergence of the difference-based scheme (assuming that P.E. is satisfied) is faster than that of the output-based scheme since $z[n]$ carries more specific information about ν^*.

The P.E. condition for the difference-based algorithm is equivalent to that $\{V[n]\}_{n=n_0}^{n_0+N-1}$ spans $\mathbb{R}^K$ since $V[n]$ can take only a finite number of possible values. It is of practical interest to express the P.E. conditions in terms of the input $u[n]$ to the hysteresis operator (in which case $u[n]$ is said to be P.E.). Recall that $u[n]$ takes values in a finite set $\{u_i, 1 \leq i \leq L+1\}$. To avoid ambiguity one should understand that the input to the Preisach operator is monotonically changed from $u[n-1]$ to $u[n]$. In the analysis below it is assumed that the input does not change more than one level during one sampling time. The assumption is not restrictive considering the rate-independence of the Preisach operator, but it helps to ease the presentation.

Theorem 3.1 (Necessary condition for P.E.) *If $\{V[n]\}$ is P.E., then there exists $N > 0$, such that for any n_0, for any $i \in \{1, 2, \cdots, L\}$, $u[n]$ achieves a local maximum at u_{i+1} or a local minimum at u_i during the time period $[n_0, n_0 + N - 1]$.*

Proof. Let's call a hysteron *active* at n if it changes state at time n. Since the input changes at most one level each time, if $u[n] > u[n-1]$, the set of active hysterons must have the form $S^+_{i,j} \triangleq \{(i,j),(i,j+1),\cdots,(i,i)\}$ for some i,j with $1 \le i \le L$ and $1 \le j \le i$ (refer to the labeling scheme in Fig. 3(a)), and the components of $V[n]$ corresponding to elements of $S^+_{i,j}$ are 2 and other components equal 0. Similarly, if $u[n] < u[n-1]$, the set of active hysterons has the form $S^-_{i,j} \triangleq \{(j,j),(j+1,j),\cdots,(i,j)\}$ for some i,j, and the components of $V[n]$ corresponding to elements of $S^-_{i,j}$ are -2 and other components equal 0.

If, for some i', $u_{i'+1}$ is not a local maximum and u'_i is not a local minimum, $S^+_{i',i'}$ or $S^-_{i',i'}$ will not become the set of active hysterons during $[n_0, n_0+N-1]$. Analysis on the Preisach plane reveals that the contribution to the output from the hysteron (i',i') cannot be isolated, and hence $\{V_n\}_{n=n_0+1}^{n_0+N-1}$ does not span $\mathbb{R}^K$. □

Remark 3.1 *From Theorem 3.1, for a Preisach operator with discretization level L, it is necessary that the input $u[n]$ has L reversals at different input levels for parameter convergence. This is in analogy to (but remarkably different from) the result for linear systems, where the input is required to have at least n frequency components for identification of n parameters [20, 21].*

Theorem 3.1 implies that the input levels u_1 and u_{L+1} must be visited for P.E. to hold. When the input hits u_1, all hysterons have output -1 and the Preisach operator is in negative saturation; similarly, when the input hits u_{L+1}, the Preisach operator is in positive saturation. For either case all the previous memory is "erased" and the operator is "reset". Starting from these reset points, one can keep track of the memory curve $\psi[n]$ (the state of the Preisach operator) according to the input $u[\cdot]$. Consider an input sequence $\{u[n]\}_{n=n_a}^{n_b}$, $n_a < n_b$. If there exist n_1, n_2, n_3 and n_4 with $n_a \le n_1 < n_2 \le n_3 < n_4 \le n_b$ such that the memory curve $\psi[n_1] = \psi[n_3]$ and $\psi[n_2] = \psi[n_4]$, we can obtain another input sequence $\{u'[n]\}_{n=n_a}^{n_b}$ by swapping the section $\{u[n]\}_{n=n_1}^{n_2}$ with the section $\{u[n]\}_{n=n_3}^{n_4}$. We write $\{u[n]\}_{n=n_a}^{n_b} \overset{P.E.}{\equiv} \{u'[n]\}_{n=n_a}^{n_b}$ (called *equivalent in terms of P.E.*) since the two sequences carry same excitation information for the purpose of parameter identification. The set of all input sequences obtained from $\{u[n]\}_{n=n_a}^{n_b}\}$ as explained above (with possibly zero or more than one swappings) form the *P.E. equivalent class* of $\{u[n]\}_{n=n_a}^{n_b}\}$, denoted as $\{\underline{u[n]}\}_{n=n_a}^{n_b}\}$. Note that in particular, $\{u[n]\}_{n=n_a}^{n_b}\} \in \{\underline{u[n]}\}_{n=n_a}^{n_b}\}$. We are now ready to present a sufficient condition for P.E. in terms of the input $u[n]$.

Theorem 3.2 (Sufficient condition for P.E.) *If there exists $N > 0$, such that for any n_0, one can find $\{u'[n]\}_{n=n_0}^{n_0+N-1} \in \{\underline{u[n]}\}_{n=n_0}^{n_0+N-1}$ satisfying the following: there exist time indices $n_0 \le n_a \le n_1^- < n_1^+ < n_2^- < n_2^+ < \cdots < n_i^- < n_i^+ < \cdots \le n_b \le n_0+N-1$ or $n_0 \le n_a \le n_1^+ < n_1^- < n_2^+ < n_2^- < \cdots < n_i^+ < n_i^- < \cdots \le n_b \le n_0+N-1$, such that $u'[n_i^+]$ is a local maximum and $u'[n_i^-]$ is a local minimum of $\{u'[n]\}_{n=n_a}^{n_b}$ for each i, these local maxima and minima include all input levels $\{u_i\}_{i=1}^{L+1}$, and either*

(a) $\{u'[n_i^+]\}$ is non-increasing, $u'[n_i^+] \ge u'[n]$ for $n_i^+ < n \le n_b$, $u'[n_i^+]$ differs from $u'[n_{i+1}^+]$ by no more than Δ_u, and $\{u'[n_i^-]\}$ is non-decreasing, $u'[n_i^-] \le u'[n]$ for $n_i^- < n \le n_b$, $u'[n_i^-]$ differs from $u'[n_{i+1}^-]$ by no more than Δ_u; or

(b) $\{u'[n_i^+]\}$ is non-decreasing, $u'[n_i^+] \le u'[n]$ for $n_i^+ < n \le n_b$, $u'[n_i^+]$ differs from $u'[n_{i+1}^+]$ by no more than Δ_u, and $\{u'[n_i^-]\}$ is non-increasing, $u'[n_i^-] \ge u'[n]$ for $n_i^- < n \le n_b$, $u'[n_i^-]$ differs from $u'[n_{i+1}^-]$ by no more than Δ_u,

then $V[n]$ corresponding to $u[n]$ is P.E.

Proof. Construct a new input sequence $\bar{u}[n]$ based on $u'[n]$ which achieves the local maxima $\{u'[n_i^+]\}$ and the local minima $\{u'[n_i^-]\}$ with the same order as in $u'[n]$, but $\bar{u}[n]$ varies monotonically from a maximum to the next minimum or from a minimum to the next maximum. For such an input, memory curve analysis on the Preisach plane reveals that the corresponding $\{\bar{V}[n]\}$ spans $\mathbb{R}^K$. From the way $\bar{u}[n]$ is constructed and the conditions given in the theorem, any vector in $\{\bar{V}[n]\}$ must also be present in $\{V'[n]\}$ corresponding to $u'[n]$. Hence $\{V'[n]\}$ is P.E. Finally P.E. of $\{V[n]\}$ follows since $\{u'[n]\}_{n=n_0}^{n_0+N-1}$ belongs to the P.E. equivalent class of $\{u[n]\}_{n=n_0}^{n_0+N-1}$. □

Theorem 3.2 is not conservative, and it covers a wide class of P.E. inputs. For example, it can be easily verified that a (periodic) first order reversal input (see Fig. 4(a) for case $L = 4$), which has been widely used for identification of Preisach density function [16], and a (periodic) oscillating input with decreasing amplitude (Fig. 4(b) for case $L = 4$) both satisfy the conditions in Theorem 3.2, and are thus P.E. In these two cases, $u[n]$ itself satisfies the conditions imposed for $u'[n]$ in the theorem. Fig. 5 shows an example where one can conclude the P.E. of a periodic $u[n]$ by inspecting a P.E. equivalent input $u'[n]$. Note that Theorem 3.2 does not require $u[n]$ to be periodic, although periodic examples are chosen here for easy illustration.

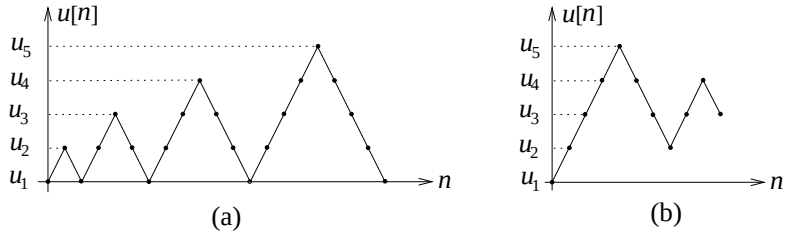

Fig. 4: Examples of P.E. inputs ($L = 4$, showing one period): (a) The first order reversal input; (b) An oscillating input with decaying amplitude.

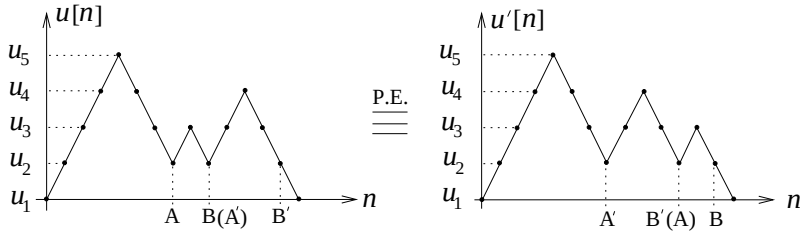

Fig. 5: An example of P.E. input ($L = 4$, showing one period). The input $u'[n]$, P.E. equivalent to $u[n]$, is obtained by swapping two sections $A - B$ and $A' - B'$ of $u[n]$.

3.3 Comparison of recursive identification schemes

In this subsection the output-based scheme is compared with the difference-based one through simulation. As shown in (8), the minimum eigenvalue of the observability grammian (i.e., c_1 in (7)) is directly related to the convergence rate of the output-based scheme. The same statement holds for the difference-based scheme provided that $W[n]$ is replaced with $V[n]$ in the related equations. In Table 1 we list the corresponding $\sqrt{1-c_1}$ (the bound on parameter error drop over one period) under the two gradient schemes (with $\gamma = 1$) for different discretization levels L with the (periodic) first order reversal input. From Table 1, the difference-based scheme converges faster

as expected. Simulation has been conducted for the case $L = 10$. Fig. 6(a) compares the decrease of parameter error over periods for the two algorithms when there is no measurement noise, and the conclusion is consistent with Table 1.

Table 1: Comparison of convergence rates for the output-based algorithm and the difference-based algorithm.

L	$\sqrt{1-c_1}$ (Output-based)	$\sqrt{1-c_1}$ (Difference-based)
5	0.9631	0.9399
10	0.9908	0.9784
15	0.9958	0.9874
20	0.9976	0.9912
25	0.9985	0.9933

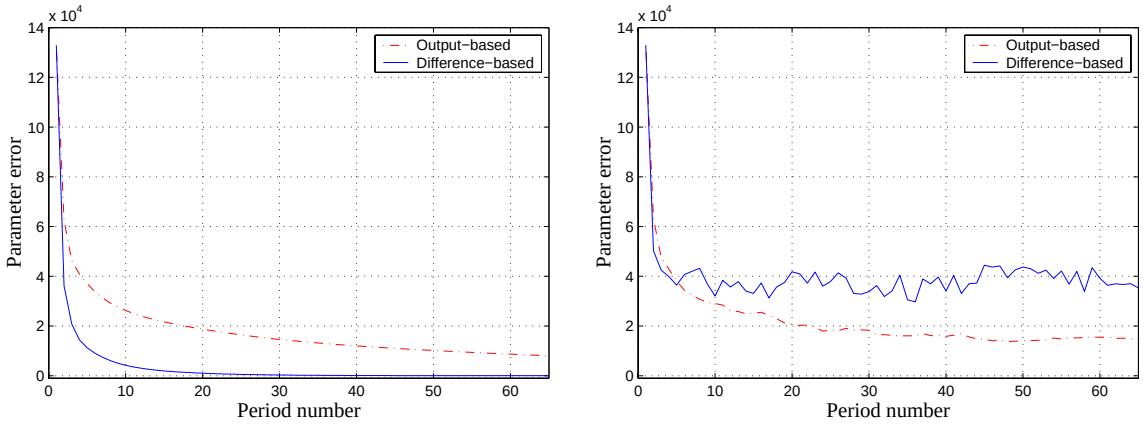

(a) (b)

Fig. 6: Comparison of parameter convergence for the output based algorithm and the difference-based algorithm. (a) Case I: noiseless measurement; (b) Case II: noisy measurement.

Despite the apparent advantage of faster convergence, the difference-based scheme is more sensitive to the measurement noise: the noise gets magnified when one takes the output difference (analogous to taking the derivative of a noisy continuous-time signal), and the disturbance is shared only among the active hysterons. Simulation in Fig. 6(a) is re-conducted where a noise is added to the output, the noise magnitude being 4% of the saturation output of the Preisach operator. From Fig. 6(b), in this case, the parameter error will not converge to zero under either of the two algorithms. However, the ultimate identification error of the output-based algorithm is much lower than that of the difference-based scheme.

3.4 Experimental results based on a magnetostrictive actuator

Having discussed the methods for recursive identification of weighting masses for a Preisach operator, we now point out how to change the previous algorithms to identify the (piecewise uniform) Preisach density directly. In

this case the input is no longer limited to a finite set of values; instead it can take any value in $[u_{min}, u_{max}]$. Each component $\bar{W}_{i,j}[n]$ of $W[n]$ no longer represents the state (1 or -1) of the hysteron at the center of the cell (i,j); instead it represents the *signed area* of the cell:

$$\bar{W}_{i,j}[n] = \text{area of } C^{+}_{i,j}[n] - \text{area of } C^{-}_{i,j}[n],$$

where $C^{\pm}_{i,j}[n] \triangleq \{(\beta,\alpha) \in \text{ cell } (i,j) : \text{ the output of } \hat{\gamma}_{\beta,\alpha} \text{ at time } n \text{ is } \pm 1\}$. The definition for $V[n]$ remains the same: $V[n] \triangleq W[n] - W[n-1]$. The P.E. conditions (Theorems 3.1 and 3.2) presented for the case of weighting masses can be extended to the case of piecewise uniform densities in a straightforward manner with minor modifications.

Experiments have been conducted on a magnetostrictive actuator to examine the identification schemes. Magnetostriction is the phenomenon of strong coupling between magnetic properties and mechanical properties of some ferromagnetic materials (e.g., Terfenol-D): strains are generated in response to an applied magnetic field, while conversely, mechanical stresses in the materials produce measurable changes in magnetization. Magnetostrictive actuators have applications to micro-positioning, robotics, ultrasonics, vibration control, etc. Fig. 7 shows a sectional view of a Terfenol-D actuator manufactured by Etrema Products, Inc. By varying the current in the coil, one varies the magnetic field in the Terfenol-D rod and thus controls the motion of the rod head. Like other smart material actuators, magnetostrictive actuators display strong input-output hysteresis [22].

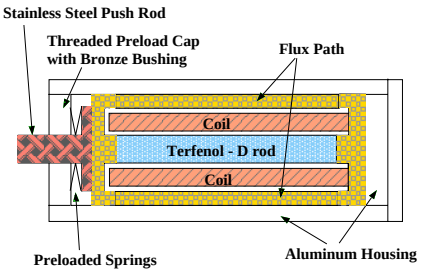

Fig. 7: Sectional view of a Terfenol-D actuator [23](Original source: Etrema Products, Inc.).

When operated in a low frequency range (typically below 5 Hz), the magnetostrictive hysteresis is rate-independent and can be modeled by (see [7])

$$\begin{cases} H = c_0 I + H_{bias} \\ M = \Gamma[H, \psi_0] \\ D = \frac{l_{rod}\lambda_s}{M_s^2} M^2 \end{cases} . \tag{10}$$

Here I is the current input and D is the displacement output. The magnetic field H along the rod direction is related to I linearly, where $c_0 > 0$ is the coil factor and H_{bias} is the bias field necessary for generating bi-directional strains. The bulk magnetization M along the rod direction is related to D via a square law, and the constants l_{rod}, λ_s, M_s denote the rod length, saturation magnetostriction and saturation magnetization, respectively. Hence the magnetostrictive hysteresis is essentially captured through the ferromagnetic hysteresis between M and H, which is modeled by the Preisach operator Γ.

In our experiments the actuator displacement is measured with a LVDT sensor, which (after low-pass filtering) has a precision of $\pm 0.5\mu$m. The DSpace ControlDesk is used to send control commands and collect data. The

following parameters are available from the manufacturer: $c_0 = 1.54 \times 10^4$/m, $M_s = 7.87 \times 10^5$A/m, $l_{rod} = 5.13 \times 10^{-2}$m, and the following parameters can be identified relatively easily: $\lambda_s = 1.3 \times 10^{-3}$, $H_{bias} = 1.12 \times 10^4$A/m. The current input is limited to the range $[-0.7\text{A}, 1.3\text{A}]$. "Practical" negative saturation M_{min} and positive saturation M_{max} can be obtained by measuring the displacements corresponding to $I = -0.7$A and 1.3A, respectively. The constant contribution to the Preisach operator (refer to the discussion in Subsection 3.1) is evaluated as $\frac{M_{min}+M_{max}}{2}$.

A periodic first order reversal current input is used for recursive identification of the Preisach density function. A practically important issue is the choice of the discretization level L for the input. Fig. 8 shows the identified density distribution for different discretization levels after eight periods. The output-based gradient algorithm is used with $\gamma = 1$.

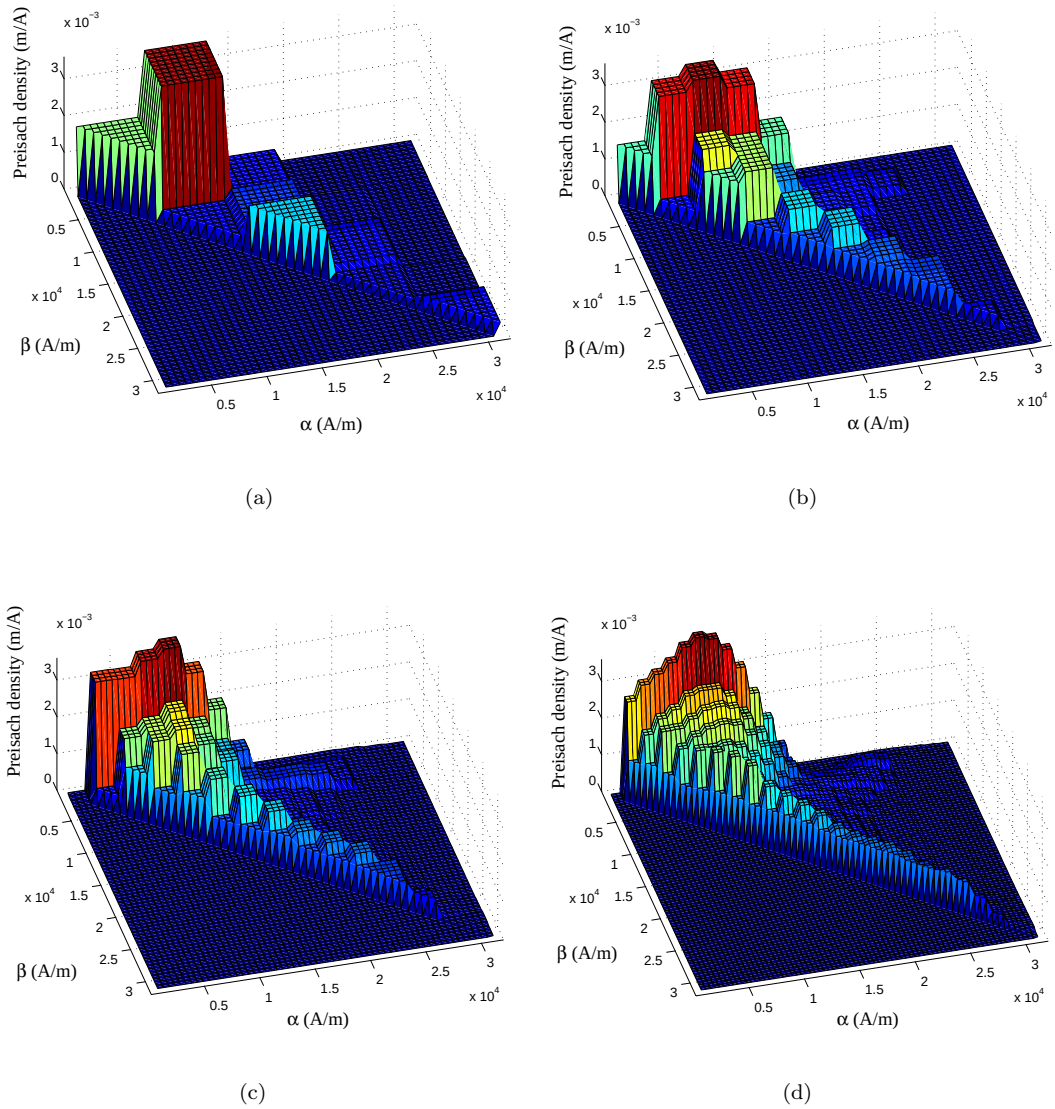

Fig. 8: The Preisach density function identified for different levels of discretization L. (a) $L = 5$; (b) $L = 10$; (c) $L = 15$; (d) $L = 25$.

Although it is expected that the higher discretization level L, the higher model accuracy, there are two factors supporting a moderate value of L in practice: the computational complexity and the sensor accuracy level. Since the number of cells on a discretization grid scales as L^2, so is the computational complexity of the recursive identification algorithm. It should also be noted that, from Table 1, the convergence rate $\sqrt{1-c_1}$ decreases as L increases. Fig. 9 shows the CPU time used in recursive identification for different discretization levels. (To obtain the CPU time, the recursive algorithm is carried out again using the collected data (the current I and the displacement D) of 8 periods on a Dell laptop Inspiron 4150.) Also shown in Fig. 9 is the CPU time it takes to compute the Preisach density function using an off-line, constrained least squares algorithm [7], where the data of one period were used. From Fig. 9, the square law for the recursive algorithm is evident. The off-line algorithm becomes prohibitively time-consuming as L gets large, due to the increasing complexity of solving a constrained optimization problem of many variables.

In the presence of the sensor noise and unmodeled dynamics, higher discretization level may not necessarily lead to improved performance. Fig. 10 compares the measured hysteresis loops against the predicted loops based on the identified parameters for different L. Although the scheme with $L = 10$ achieves much better match than the scheme with $L = 5$, there is little improvement when L is increased to 15. Hence for the Terfenol-D actuator (and the sensor used), it is determined that $L = 10$ is an appropriate discretization level for the Preisach operator.

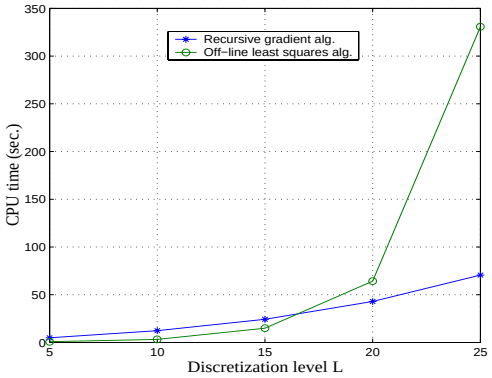

Fig. 9: CPU time used in the recursive gradient algorithm and the off-line least squares algorithm.

4 Adaptive Inverse Control

Fig. 11 shows a schematic of adaptive inverse control. The input to the Preisach operator is obtained through inversion of the Preisach operator $\hat{\Gamma}$ with the current estimate of the Preisach density. The error between the reference trajectory and the achieved trajectory is then used to update the parameter estimate and thus the inverse model. For a Preisach operator with piecewise uniform density, its exact right inverse can be efficiently constructed [13]. Note that for the Preisach operator Γ (with a piecewise uniform density function) to have a unique (right) inverse, it is required that all diagonal cells have strictly positive density values [17]. However, when a particular inversion algorithm (e.g., the one in [13]) is used, the inverse trajectory can be made unique even if some diagonal density values are zero.

To the authors' best knowledge, the parameter convergence issue in adaptive inverse control of hysteresis has

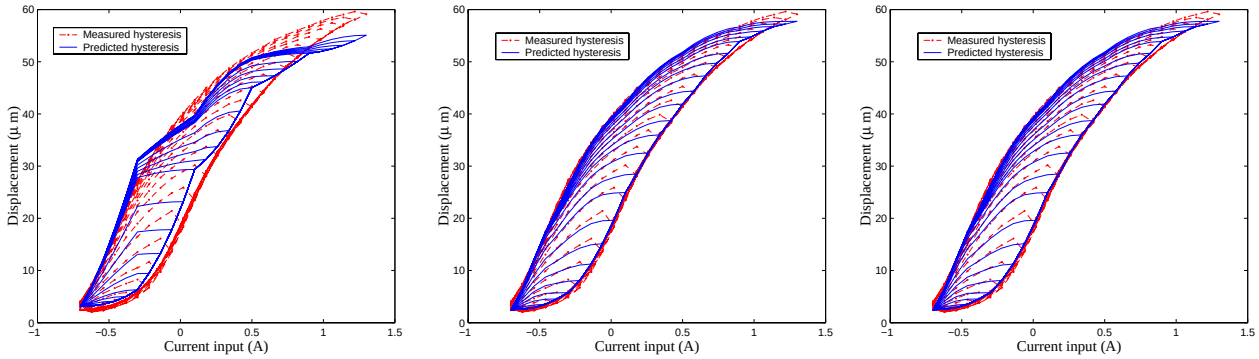

(a) (b) (c)

Fig. 10: Comparison of measured hysteresis loops with predicted loops based on the identified Preisach density function. (a) $L = 5$; (b) $L = 10$; (c) $L = 15$.

not been studied in literature. In this section we aim to answer the following question: how is the parameter convergence related to the reference trajectory?

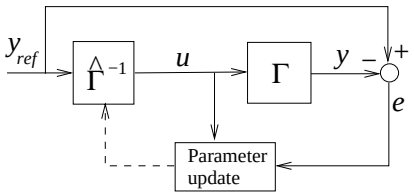

Fig. 11: A schematic of adaptive inverse control.

Theorem 4.1 *Assume that the true Preisach operator has a piecewise uniform density function, as illustrated in Fig. 3 (a). Denote by ν^* the K-dimensional vector of true densities, and by y_{sat} the saturation output corresponding to ν^*. Let the output-based gradient algorithm be used for the parameter update. Then*

(1) For any reference trajectory $y_{ref}[\cdot]$ with $y_{ref}[n] \in [-y_{sat}, y_{sat}]$, the parameter estimate $\hat{\nu}[n] \to \hat{\nu}_\infty$ for some $\hat{\nu}_\infty$, and the tracking error $e[n] = y[n] - y_{ref}[n] \to 0$ as $n \to \infty$;

(2) Assume that the density $\bar{\nu}_{1,1}$ of the cell $(1,1)$ is positive. Let $y_{ref}[\cdot]$ be periodic of period N that visits $-y_{sat}$, and without loss of generality $y_{ref}[1] = -y_{sat}$. Define $u_r[n] \triangleq \Gamma^{-1}[y_{ref}[\cdot], \psi_0][n]$ with ψ_0 the memory curve corresponding to the negative saturation, where Γ^{-1} is as constructed in [13]. Then $u_r[\cdot]$ is also periodic with period N, and $u_r[1] = u_{min}$. Let the vector of signed areas of cells corresponding to $u_r[\cdot]$ be $W_r[\cdot]$ (which is also periodic), and the null space of $[W_r[1] \cdots W_r[N]]^T$ be $\mathcal{N}_r$. Then the parameter estimate $\hat{\nu}[n] \to \mathcal{N}_r + \nu^* \triangleq \{x + \nu^* : x \in \mathcal{N}_r\}$. In particular, if $\{W_r[n]\}_{n=1}^N$ spans $\mathbb{R}^K$, $\hat{\nu}[n] \to \nu^*$. Analogous results hold if $\bar{\nu}_{L,L} > 0$ and $y_{ref}[\cdot]$ visits y_{sat}.

Proof. (1) Define $\tilde{\nu}[n] \triangleq \hat{\nu}[n] - \nu^*$, and $\delta[n] \triangleq \tilde{\nu}[n]^T \tilde{\nu}[n]$. From the output-based gradient algorithm (letting $\gamma = 1$

without loss of generality),

$$\begin{aligned}\delta[n+1] &= \delta[n] - \frac{\tilde{\nu}[n]^T W[n] W[n]^T \tilde{\nu}[n]}{W[n]^T W[n]} \\ &= \delta[n] - \frac{(y[n]-\hat{y}[n])^2}{W[n]^T W[n]} \leq \delta[n]. \end{aligned} \tag{11}$$

Since $\delta[n] \geq 0$, $\delta[n] \to \delta_\infty$ as $n \to \infty$. This immediately results in $\hat{\nu}[n] \to \hat{\nu}_\infty$ for some $\hat{\nu}_\infty$. Summing (11) over n leads to

$$\sum_{n=0}^{\infty} \frac{(y[n]-\hat{y}[n])^2}{W[n]^T W[n]} = \delta[0] - \delta_\infty < \infty,$$

which implies $\frac{(y[n]-\hat{y}[n])^2}{W[n]^T W[n]} \to 0$. Since $W[n]^T W[n] < C$ for some constant C,

$$|y[n] - \hat{y}[n]| \to 0, \text{ as } n \to \infty. \tag{12}$$

The Preisach operator $\hat{\Gamma}$ based on parameter estimate at n can be exactly inverted (hence $\hat{y}[n] = y_{ref}[n]$) except for the following two cases: (a) $\hat{y}_{sat}[n] < y_{ref}[n] \leq y_{sat}$, and (b) $-y_{sat} \leq y_{ref}[n] < -\hat{y}_{sat}[n]$, where $\hat{y}_{sat}[n]$ denotes the saturation output corresponding to $\hat{\nu}[n]$. For the case (a), the inversion cannot be exact and the input under the inversion algorithm is $u[n] = u_{max}$ (so that the corresponding $\hat{y}[n]$ is *closest* to $y_{ref}[n]$), which implies $\hat{y}[n] = \hat{y}_{sat}[n]$, $y[n] = y_{sat}$, and hence $|y[n] - y_{ref}[n]| < |y[n] - \hat{y}[n]|$. The same conclusion holds for the case (b). It then follows from (12) that the tracking error $e[n] = y[n] - y_{ref}[n]$ approaches 0 as $n \to \infty$.

(2) Since $y_{ref}[kN+1] = -y_{sat}$ for each k and $\bar{\nu}_{1,1} > 0$, $u_r[kN+1] = u_{min}$ and the state of the Preisach operator is reset at $kN+1$. The periodicity of $u_r[\cdot]$ then follows from that of $y_{ref}[\cdot]$ and the inverse algorithm. From the first part of the theorem, $|y[n] - y_{ref}[n]| \to 0$ and hence $y[kN+1] \to -y_{sat}$ as $k \to \infty$. Again from $\bar{\nu}_{1,1} > 0$, the input $u[kN+1]$ approaches u_{min} as $k \to \infty$, and $u[kN+m] \to u_r[m]$ for $1 \leq m \leq N$. As a consequence, $W[kN+m] \to W_r[m]$. Since as $k \to \infty$

$$W[kN+m]^T \tilde{\nu}[kN+m] \to 0, \text{ for } 1 \leq m \leq N,$$

we conclude $W_r[m]^T \hat{\nu}_\infty = W_r[m]^T \nu^*$, $1 \leq m \leq N$, i.e., $\hat{\nu}_\infty \in \mathcal{N}_r + \nu^*$. Analogous arguments can be used for the case where $\bar{\nu}_{L,L} > 0$ and $y_{ref}[\cdot]$ visits y_{sat}. □

Simulation has been conducted to illustrate Theorem 4.1. Fig. 12 shows the simulation result of tracking a sinusoidal signal with amplitude y_{sat} using the output-based adaptive inverse scheme. One can see that the tracking error goes to zero. Fig. 13 compares the parameter estimate after 160 periods with the true parameter values. Note that the individual density values do not converge (Fig. 13(a)). For this particular reference trajectory, the asymptotic input will be periodic varying between u_{min} and u_{max} without other reversals. Hence for each i the signed areas of cells $(i,1), \cdots, (i,i-1)$ will be the same; and for each j, the signed areas of cells $(j+1,j), \cdots, (L,j)$ will be the same. What separates a diagonal cell from other cells of the row (or the column) is its triangular shape. As a result, one can predict that the densities of diagonal cells will be correctly identified and the sum of densities of cells in each row (or column) (excluding the diagonal element) will be correctly identified. This is verified in Fig. 13(b).

Experimental results for tracking a sinusoidal signal are shown in Fig. 14 with two different adaptation constants γ. When γ is bigger, the trajectory converges to the steady state faster but with larger tracking error due to higher sensitivity to the noise. For $\gamma = 0.2$, the tracking error is under 1 μm. Considering the sensor precision, almost

perfect tracking is achieved for the full operational range of the actuator (Fig. 15). In these experiments and other experiments reported hereafter, the discretization level $L = 10$.

If the reference trajectory does not cover $\pm y_{sat}$, Theorem 4.1 says that the tracking error still goes to zero, but one cannot say more about the parameter convergence. In this case there is no reset mechanisms during the adaptation, and depending on the initial conditions of the system and the adaptation process, the final steady-state input trajectories can be different (while the output trajectories are all consistent with the reference trajectory). Essentially in this case there may exist multiple minor loops that satisfy the output requirement. This is also demonstrated by experiments (Fig. 16), where two different inputs are found to achieve tracking of a sinusoidal trajectory with amplitude 15μm (and a DC offset of 30μm).

We note that in Theorem 4.1 the output-based algorithm is required. The results cannot be extended to the difference-based algorithm. Indeed it has been verified that the difference-based adaptive inverse scheme cannot achieve asymptotic tracking (Fig. 17).

5 Conclusions

This paper has been focused on recursive identification and adaptive inverse control of hysteresis in smart materials. A Preisach operator with piecewise uniform density function was used to approximate smart material hysteresis. On the theoretical side, a necessary condition and a sufficient condition for the parameter convergence were presented in terms of the input to the Preisach operator. In contrast to the results for linear systems, the conditions here center around the local maxima/minima of the input. Asymptotic tracking under the output-based algorithm was established, and the issue of parameter convergence was discussed in terms of the reference trajectory.

Practical issues of using the adaptive schemes were studied in depth, through both simulation and experiments. Two types of adaptive gradient identification algorithms were compared. It was found that, for purely recursive identification (i.e., given the same input), the difference-based method has a higher convergence rate in the absence of noise, but it is more sensitive to the measurement noise. On the other hand, for tracking with adaptive inverse control, the difference-based scheme is not usable. The choice of the level of discretization was also discussed. It was shown that a moderate L can be used, taking into account the factors of computational cost, sensing precision, and model accuracy. In particular, experimental results have shown that the adaptive scheme is able to virtually cancel out the hysteresis effect throughout the actuator working range with $L = 10$ for our experimental setup. Most results of this paper are applicable if the adaptive least squares algorithms [20, 21] (instead of the gradient algorithms) are used for parameter update.

For future work, it will be of interest to extend the results reported here to the cases where the hysteresis output is not directly measurable. Such cases happen if, e.g., the high-frequency dynamics of the smart material actuator is not negligible [13], or the actuator is used to control some other plant.

References

[1] S. O. R. Moheimani and G. C. Goodwin, "Guest editorial introduction to the special issue on dynamics and control of smart structures," *IEEE Transactions on Control Systems Technology*, vol. 9, no. 1, pp. 3–4, 2001.

[2] A. A. Adly, I. D. Mayergoyz, and A. Bergqvist, "Preisach modeling of magnetostrictive hysteresis," *Journal of Applied Physics*, vol. 69, no. 8, pp. 5777–5779, 1991.

[3] D. Hughes and J. T. Wen, "Preisach modeling and compensation for smart material hysteresis," in *Active Materials and Smart Structures*, G. L. Anderson and D. C. Lagoudas, Eds., 1994, vol. 2427 of *SPIE*, pp. 50–64.

[4] J. Schäfer and H. Janocha, "Compensation of hysteresis in solid-state actuators," *Sensors and Actuators A*, vol. 49, no. 1-2, pp. 97–102, 1995.

[5] P. Ge and M. Jouaneh, "Tracking control of a piezoceramic actuator," *IEEE Transactions on Control Systems Technology*, vol. 4, no. 3, pp. 209–216, 1996.

[6] R. B. Gorbet, D. W. L. Wang, and K. A. Morris, "Preisach model identification of a two-wire SMA actuator," in *Proceedings of IEEE International Conference on Robotics and Automation*, 1998, pp. 2161–2167.

[7] X. Tan, R. Venkataraman, and P. S. Krishnaprasad, "Control of hysteresis: Theory and experimental results," in *Modeling, Signal Processing, and Control in Smart Structures*, V. S. Rao, Ed., 2001, vol. 4326 of *SPIE*, pp. 101–112.

[8] D. Croft, G. Shed, and S. Devasia, "Creep, hysteresis, and vibration compensation for piezoactuators: atomic force microscopy application," *Journal of Dynamic Systems, Measurement, and Control*, vol. 123, no. 1, pp. 35–43, 2001.

[9] H. T. Banks, A. J. Kurdila, and G. Webb, "Identification of hysteretic control influence operators representing smart actuators, Part I: Formulation," *Mathematical Problems in Engineering*, vol. 3, no. 4, pp. 287–328, 1997.

[10] W. S. Galinaitis and R. C. Rogers, "Control of a hysteretic actuator using inverse hysteresis compensation," in *Mathematics and Control in Smart Structures*, V.V. Varadan, Ed., 1998, vol. 3323 of *SPIE*, pp. 267–277.

[11] G. Tao and P. V. Kokotović, "Adaptive control of plants with unknown hysteresis," *IEEE Transactions on Automatic Control*, vol. 40, no. 2, pp. 200–212, 1995.

[12] R. C. Smith, "Inverse compensation for hysteresis in magnetostrictive transducers," Tech. Rep. CRSC-TR98-36, CRSC, North Carolina State University, 1998.

[13] X. Tan and J. S. Baras, "Modeling and control of hysteresis in magnetostrictive actuators," *Automatica*, 2003, provisionally accepted (revised), available at `http://www.isr.umd.edu/~xbtan/papers.html`.

[14] G. V. Webb, D. C. Lagoudas, and A. J. Kurdila, "Hysteresis modeling of SMA actuators for control applications," *Journal of Intelligent Materials Systems and Structures*, vol. 9, no. 6, pp. 432–448, 1998.

[15] K. Kuhnen and H. Janocha, "Adaptive inverse control of piezoelectric actuators with hysteresis operators," in *Proceedings of European Control Conference (ECC)*, Karsruhe, Germany, 1999, Paper F 0291.

[16] I. D. Mayergoyz, *Mathematical Models of Hysteresis*, Springer Verlag, 1991.

[17] A. Visintin, *Differential Models of Hysteresis*, Springer, 1994.

[18] M. Brokate and J. Sprekels, *Hysteresis and Phase Transitions*, Springer Verlag, New York, 1996.

[19] K.-H. Hoffmann, J. Sprekels, and A. Visintin, "Identification of hysteretic loops," *Journal of Computational Physics*, vol. 78, pp. 215–230, 1988.

[20] G. C. Goodwin and K. S. Sin, *Adaptive Filtering, Prediction and Control*, Prentice-Hall, Inc., Englewood Cliffs, NJ, 1984.

[21] S. Sastry and M. Bodson, *Adaptive Control: Stability, Convergence, and Robustness*, Prentice Hall, Englewood Cliffs, NJ, 1989.

[22] X. Tan, *Control of Smart Actuators*, Ph.D. thesis, University of Maryland, College Park, MD, 2002, available as ISR Technical Report PhD 2002-8 at `http://techreports.isr.umd.edu/ARCHIVE`.

[23] R. Venkataraman, *Modeling and Adaptive Control of Magnetostrictive Actuators*, Ph.D. thesis, University of Maryland, College Park, 1999.

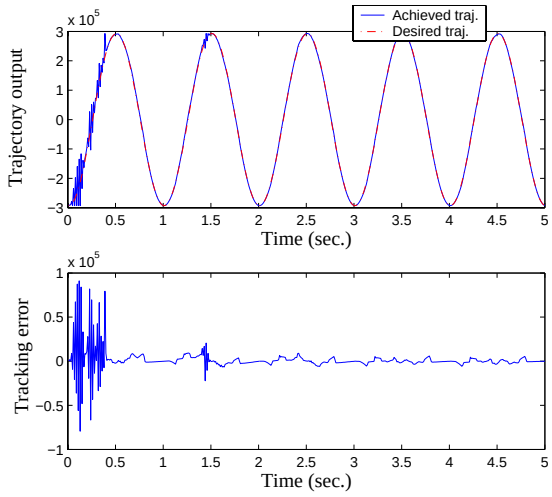

Fig. 12: Simulation result of adaptively tracking a sinusoidal signal with amplitude y_{sat} ($L = 10$).

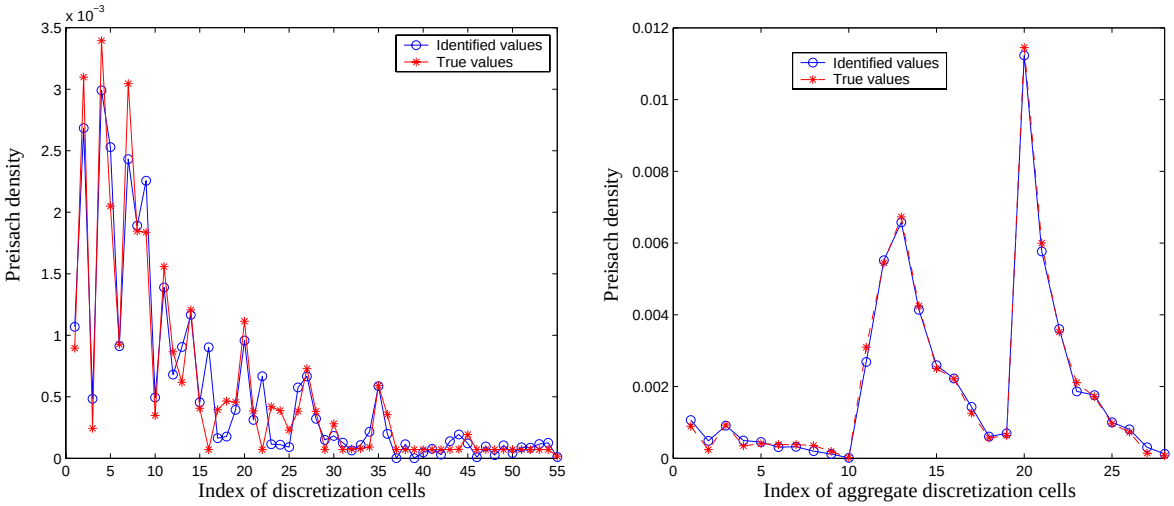

(a) (b)

Fig. 13: Comparison of identified parameter values with true values $L = 10$: (a) Comparison for individual cell density values; (b) Comparison for *aggregate* cell density values.

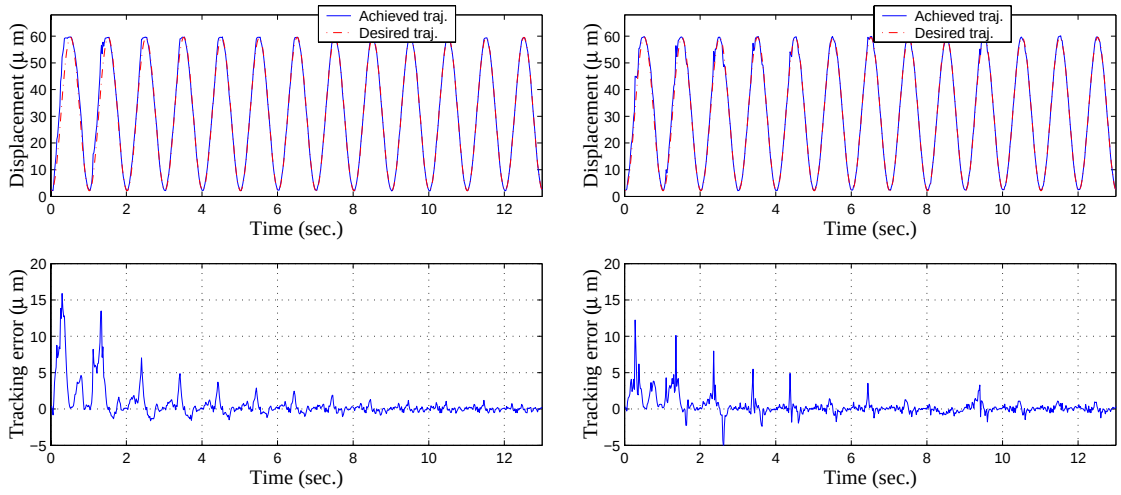

(a) (b)

Fig. 14: Experimental results of tracking a sinusoidal reference trajectory: (a) $\gamma = 0.2$; (b) $\gamma = 0.5$.

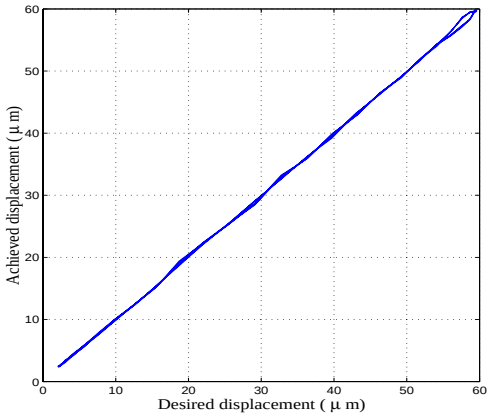

Fig. 15: Achieved displacement *vs.* desired displacement (over the full operational range of the actuator).

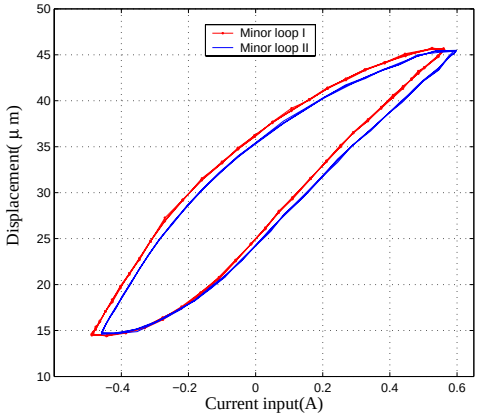

Fig. 16: Two minor loops corresponding to tracking a sinusoidal signal with amplitude less than y_{sat}.

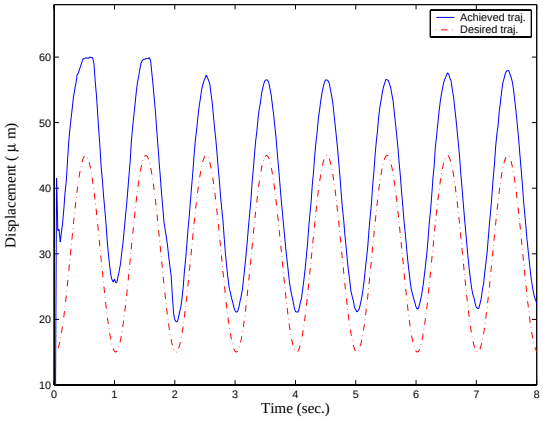

Fig. 17: Experimental result showing that the difference-based adaptive scheme cannot achieve asymptotic tracking.